

Topological Magnons on the Ferromagnetic Zigzag Lattice

Skandan Subramanian,^{1,2,*} Tom Berlijn,³ Lucas Lindsay,¹ Randy S. Fishman,¹ and John W. Villanova^{4,†}

¹*Materials Science and Technology Division, Oak Ridge National Laboratory, Oak Ridge, Tennessee 37831, USA*

²*Department of Physics, Indian Institute of Technology, Madras, India*

³*Center for Nanophase Materials Sciences, Oak Ridge National Laboratory, Oak Ridge, Tennessee 37831, USA*

⁴*Department of Physics and Astronomy, Middle Tennessee State University, Murfreesboro, Tennessee 37132, USA*

(Dated: November 28, 2024)

Motivated by the experimental identification of magnetic compounds consisting of zigzag chains, we analyze the band structure topology of magnons in ferromagnets on a zigzag lattice. We account for the general lattice geometry by including spatially anisotropic Heisenberg exchange interactions and by Dzyaloshinskii-Moriya interaction on inversion asymmetric bonds. Within the linear spin-wave theory, we find two magnon branches, whose band structure topology (i.e., Chern numbers) we map out in a comprehensive phase diagram. Notably, besides topologically trivial and gapless phases, we identify topologically nontrivial phases that support chiral edge magnons. We show that these edge states are robust against elastic defect scattering.

I. INTRODUCTION

Topology has become a critical topic in condensed matter physics [1–3]. Topological edge states have drawn significant attention due to their potential for enabling dissipationless and robust channels for information transfer [4–7]. Recently the concept of topological band structures has been extended to the elementary excitations of magnetically ordered insulators, magnons. Magnonic topological insulators, characterized by nontrivial topological invariants, have been predicted [3, 8–10]. A major experimental challenge lies in directly detecting topological edge states, as neutron scattering cannot capture their signature. Thus local spectroscopic probes and transport measurements are important signatures: these topological materials exhibit the magnon Hall [11–16] and Seebeck [17, 18] effects due to their Berry curvature, which can be considered as a fictitious magnetic field in momentum space [19–21].

The identification of suitable material candidates remains a critical bottleneck. Honeycomb lattice van der Waals magnets represent some of the most prominent current examples of potential magnon Chern insulators [10, 22–24]. Unfortunately, many of these materials are highly air-sensitive which complicates experimental studies. Expanding the class of materials capable of hosting magnon Chern insulators with chiral edge states is therefore an urgent priority for advancing the field. Previous

studies have demonstrated that magnon Chern insulators can be realized in ferromagnets on various lattice geometries, including the pyrochlore [11, 12], kagome [25], star [26], and honeycomb [27–29] lattices. Recently, the zigzag lattice has also been identified as a platform with promising topological properties of magnons [30]. In this work, we conduct a detailed analysis of the topological properties of magnons in zigzag lattice ferromagnets. We derive analytic conditions for the exchange interactions that enable topologically nontrivial magnon phases. Furthermore, we investigate the robustness of chiral edge states against disorder. Our findings contribute to broadening the set of candidate materials for realizing magnon Chern insulators, thereby paving the way for future experimental and theoretical exploration.

The structure of the ferromagnetic (FM) zigzag lattice is sketched in Fig. 1, which has alternating black and red bonds with exchange couplings $J_{1\alpha}$ and $J_{2\alpha}$, respectively, where the $\alpha \in \{x, y\}$ exchanges can be different. We define

$$r = \frac{J_{2x} + J_{2y}}{J_{1x} + J_{1y}}, \quad (1)$$

so that the directionally-averaged $J_2 > 0$ is larger than the directionally-averaged $J_1 > 0$ when $r > 1$. Several candidate FM zigzag materials have been identified: spin-1/2 Heisenberg vanadium chains in CdVO_3 [31, 32], spin-3/2 chromium chains in LaCrOS_2 [33], and spin-3.4/2 manganese chains in La_3MnAs_5 [34]. In all of these materials $r > 1$. For CdVO_3 [31, 32], $J_2 \approx 90$ K and $J_1 \approx 18$ K so that $r \approx 5$. For La_3MnAs_5 [34], $r \approx 7.6$. Similarly, r is also believed to be large in LaCrOS_2 [33]. However, the magnitude of the anisotropy $\xi_1 = J_{1x}/J_{1y}$ and $\xi_2 = J_{2x}/J_{2y}$ in these materials is unknown.

As we shall see, the topological properties in this lattice are controlled by the relative sizes of the exchange parameters. These properties include the size of the gap (if any) between the magnonic bands and the Chern numbers of the bands (either $C_n = \pm 1$ or $C_n = 0$). Associated with the Chern numbers are the number of edge modes on a ribbon constructed from the material [35–39]. Strain can

* This manuscript has been authored in part by UT-Battelle, LLC, under contract DE-AC05-00OR22725 with the US Department of Energy (DOE). The US government retains and the publisher, by accepting the article for publication, acknowledges that the US government retains a nonexclusive, paid-up, irrevocable, worldwide license to publish or reproduce the published form of this manuscript, or allow others to do so, for US government purposes. DOE will provide public access to these results of federally sponsored research in accordance with the DOE Public Access Plan (<http://energy.gov/downloads/doe-public-access-plan>)

† john.villanova@mtsu.edu

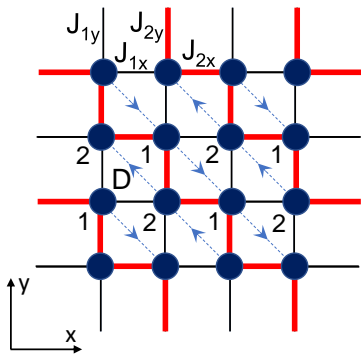


FIG. 1. A FM zigzag lattice with four different exchange parameters. The DM interaction $-D(\mathbf{S}_i \times \mathbf{S}_j) \cdot \mathbf{z}$ lies along the $(1, -1)$ diagonals with the arrows in the figure pointing from \mathbf{S}_i to \mathbf{S}_j .

be used to conveniently control the anisotropy of the exchange parameters and the topological properties of FM zigzag lattice materials.

II. MODEL AND METHOD

Because $J_{1\alpha} \neq J_{2\alpha}$, inversion symmetry is broken across the diagonals $[1, -1]$ of Fig. 1. Traversing such a diagonal, the environment to the upper right (consisting of $J_{2\alpha}$ bonds) is different from the environment to the lower left (consisting of $J_{1\alpha}$ bonds). Due to this broken inversion symmetry, Dzyaloshinskii-Moriya (DM) interactions can couple the spins on either end of the diagonal dashed lines. We denote this interaction by D and the interaction by $-D(\mathbf{S}_i \times \mathbf{S}_j) \cdot \mathbf{z}$.

Broken inversion symmetry also allows another DM interaction D' along $[1, 1]$ between neighboring red chains, but this interaction is generally weaker than D (because it involves inversion symmetry broken over larger distances in real materials) and only serves to complicate the model.

The Hamiltonian of the FM zigzag lattice is then given by

$$\mathcal{H} = -\frac{1}{2} \sum_{i,j} J_{ij} \mathbf{S}_i \cdot \mathbf{S}_j - D \sum_{i,j} (\mathbf{S}_i \times \mathbf{S}_j) \cdot \mathbf{z} - K \sum_i (\mathbf{S}_i \cdot \mathbf{z})^2, \quad (2)$$

where $K > 0$ is a single-ion anisotropy that tends to align the spins along the z -axis. Notice that there are two different magnetic sites in each unit cell. The DM interaction D couples the spin on one type of magnetic site to the spin on the same type of magnetic site in neighboring unit cells (1 to 1 or 2 to 2), whereas the exchange interactions, J_{ij} , couple nearest-neighbor sites of two different types (1 to 2).

We map the spin operators to Boson operators by means of the Holstein-Primakoff transformation: $S_{iz} = S - a_i^\dagger a_i$, $S_{i+} = S_{ix} + iS_{iy} = \sqrt{2S}a_i$, and $S_{i-} = S_{ix} - iS_{iy} = \sqrt{2S}a_i^\dagger$. The Hamiltonian is rewritten in this new form as

$$\mathcal{H} = \sum_{\mathbf{k}} \underline{v}(\mathbf{k})^\dagger \cdot \underline{H}(\mathbf{k}) \cdot \underline{v}(\mathbf{k}), \quad (3)$$

$$\underline{v}(\mathbf{k}) = \begin{pmatrix} a_{\mathbf{k}}^{(1)} \\ a_{\mathbf{k}}^{(2)} \end{pmatrix}, \quad (4)$$

$$\underline{H}(\mathbf{k}) = \frac{J_t S}{2} \begin{pmatrix} A_{\mathbf{k}}^- & -\Psi_{\mathbf{k}}^* \\ -\Psi_{\mathbf{k}} & A_{\mathbf{k}+} \end{pmatrix}, \quad (5)$$

where

$$A_{\mathbf{k}}^\pm = 1 \pm d\tau_{\mathbf{k}} + \kappa, \quad (6)$$

$$J_t = J_{1x} + J_{1y} + J_{2x} + J_{2y}, \quad (7)$$

$$\Psi_{\mathbf{k}} = \frac{J_{1x} + J_{1y}e^{i(k_x - k_y)a} + J_{2x}e^{2ik_x a} + J_{2y}e^{i(k_x + k_y)a}}{J_t}, \quad (8)$$

$d = -4D/J_t$, $\kappa = 2K/J_t$, and $\tau_{\mathbf{k}} = \sin((k_y - k_x)a)$.

As found earlier [30], the excitation frequencies are

$$\hbar\omega_1(\mathbf{k}) = J_t S (1 - \mu_{\mathbf{k}} + \kappa), \quad (9)$$

$$\hbar\omega_2(\mathbf{k}) = J_t S (1 + \mu_{\mathbf{k}} + \kappa), \quad (10)$$

where

$$\mu_{\mathbf{k}} = \sqrt{|\Psi_{\mathbf{k}}|^2 + (d\tau_{\mathbf{k}})^2}. \quad (11)$$

Notice that the only role of the anisotropy is to shift the excitation frequencies upwards by $2KS$.

The first Brillouin zone (BZ) of the FM zigzag lattice is a diamond constructed by the lines $k_x - k_y = \pm\pi/a$ and $k_x + k_y = \pm\pi/a$. For the isotropic model with $\xi_1 = \xi_2 = 1$, we find that $\tau_{\mathbf{k}} = 0$, $\Psi_{\mathbf{k}} = 0$, $\mu_{\mathbf{k}} = 0$, and $\omega_1(\mathbf{k}) = \omega_2(\mathbf{k})$ at the boundary $k_x - k_y = \pm\pi/a$. The system is gapless. When the model is anisotropic with $\xi_1 \neq 1$ or $\xi_2 \neq 1$, then $\tau_{\mathbf{k}}$ still vanishes at this boundary of the first BZ but $\Psi_{\mathbf{k}}$ and $\mu_{\mathbf{k}}$ do not, and the modes are non-degenerate except possibly at isolated \mathbf{k} points along $k_x - k_y = \pm\pi/a$. The system is generically gapped and insulating except possibly at isolated \mathbf{k} points for certain values of the exchange parameters.

We comment at this stage that the Hamiltonian we have defined here differs slightly from that in Ref. [30] in the phase factors appearing in $\Psi_{\mathbf{k}}$. This amounts to the difference, familiar to electronic tight-binding models, between phase factors relating hopping between unit cells, $e^{-i\mathbf{k} \cdot \mathbf{R}}$, versus including information about the specific site, \mathbf{z}_j , within a unit cell, $e^{-i\mathbf{k} \cdot (\mathbf{R} + \mathbf{z}_j)}$. The former

is widely used since there is no effect on the eigenvalues of the problem and one need only retain a record of which unit cell is the endpoint for the hopping (e.g. Wannier90 [40]). However, the site-discerning phase factor is sometimes favored (e.g. PythTB [41]), and defining the Hamiltonian this way ensures that the surface mapped by $\mathbf{h}(\mathbf{k})$ (defined next) is closed upon scanning the first BZ only once.

We now derive a condition for the bulk system to be a Chern insulator with nonzero Chern numbers C_n for the two magnon bands. We write the Hamiltonian matrix in Eq. (5) in the Pauli matrix basis

$$\underline{H}(\mathbf{k}) = \mathbf{h}(\mathbf{k}) \cdot \underline{\sigma} + h_0(\mathbf{k})\underline{I}, \quad (12)$$

where $\mathbf{h}(\mathbf{k})$ is a vector, $\underline{\sigma}$ the vector of 2×2 Pauli matrices, and \underline{I} is the 2×2 identity matrix. The problem is mapped to a form well-suited for analysis of the topology; we follow the geometrical approach that was applied in Ref. [42] to solve the Haldane model [43]. Solving for $\mathbf{h}(\mathbf{k})$, we find

$$h_x(\mathbf{k}) = -\frac{1}{J_t} \left(J_{1x} + J_{1y} \cos((k_x - k_y)a) + J_{2x} \cos(2k_x a) + J_{2y} \cos((k_x + k_y)a) \right), \quad (13)$$

$$h_y(\mathbf{k}) = -\frac{1}{J_t} \left(J_{1y} \sin((k_x - k_y)a) + J_{2x} \sin(2k_x a) + J_{2y} \sin((k_x + k_y)a) \right), \quad (14)$$

and

$$h_z(\mathbf{k}) = \frac{4D}{J_t} \sin((k_y - k_x)a). \quad (15)$$

Our results do not depend on $h_0(\mathbf{k})$, which acts like a chemical potential, so long as it is small enough not to close the gap anywhere in the BZ. The overall scale factor of $J_t S/2$ is not relevant to discussion of the topology.

III. DISCUSSION

A. Topology of the Bulk Hamiltonian

The eigenvalues of $\underline{H}(\mathbf{k})$ are $\pm|\mathbf{h}(\mathbf{k})|$, which agrees with the excitation frequencies in Eqs. (9) and (10). Adopting a similar methodology to that in Ref. [42], we calculate the Chern number of the lower positive frequency band as half the number of intersections of a line through the origin with the \mathbf{h} -surface. A nontrivial Chern number is obtained only if $\mathbf{h}(\mathbf{k})/|\mathbf{h}(\mathbf{k})|$ completely covers the Bloch sphere \mathbb{S}^2 and a smooth function cannot connect every point on \mathbb{S}^2 to a specific eigenvector without producing discontinuities at the poles. On the other hand, a trivial topology occurs if the sphere \mathbb{S}^2 is not fully covered

because we can then define a single map from parameter space to each eigenvector. Either way, the topology is quantified by calculating the Chern number.

The Chern number is given by the expression

$$C = \frac{1}{2} \sum_{\mathbf{k} \in \mathbb{D}} \text{sgn}(h_z(\mathbf{k})) \text{sgn} \left(\left(\frac{\partial \mathbf{h}(\mathbf{k})}{\partial k_x} \times \frac{\partial \mathbf{h}(\mathbf{k})}{\partial k_y} \right) \cdot \mathbf{z} \right), \quad (16)$$

where \mathbb{D} is the set of solutions to the equations $h_x(\mathbf{k}) = h_y(\mathbf{k}) = 0$ while demanding $h_z(\mathbf{k}) \neq 0$. The normal vector $\mathbf{n}(\mathbf{k})$ to the \mathbf{h} -surface is defined as

$$\mathbf{n}(\mathbf{k}) = \frac{\partial \mathbf{h}(\mathbf{k})}{\partial k_x} \times \frac{\partial \mathbf{h}(\mathbf{k})}{\partial k_y}. \quad (17)$$

Because both partial derivatives $\partial \mathbf{h}(\mathbf{k})/\partial k_x$ and $\partial \mathbf{h}(\mathbf{k})/\partial k_y$ are tangential to the surface, the cross product $\mathbf{n}(\mathbf{k})$ is normal to the surface. Implicit in our system of equations is choosing the h_z -axis as the line of intersection for the \mathbf{h} -surface. Such intersections with the h_z -axis are considered to be positive if $\mathbf{n}(\mathbf{k})$ and $h_z(\mathbf{k})$ have the same sign and negative otherwise. Alternatively, one may look only along a $+h_z$ -ray and neglect the factor of one-half in Eq. 16. The Chern number is nontrivial if the origin is fully enclosed by the \mathbf{h} -surface (is interior to the surface). Similar to the winding number of a curve on a plane, the result does not depend on the choice of the line mentioned above.

With the definitions $A = J_{1x} - J_{2x}$, $B = J_{1y} - J_{2y}$, $F = -(J_{1x} + J_{2x})$, and $G = -(J_{1y} + J_{2y})$, we solve the system of equations for the condition for $\mathbf{k} \in \mathbb{D}$:

$$k_x a = \arctan \left[\mp \frac{B}{G} \sqrt{\frac{G^2 - F^2}{A^2 - B^2}} \right], \quad (18)$$

$$k_y a = -\arctan \left[\pm \frac{A}{F} \sqrt{\frac{G^2 - F^2}{A^2 - B^2}} \right], \quad (19)$$

where the upper sign and lower sign are chosen simultaneously for each (k_x, k_y) pair. There are four solutions to the system of equations: one is within and one is outside the first BZ, and the other two solutions are $(-k_x, -k_y)$ in either of these cases. The set \mathbb{D} is composed of only those two solutions inside the first BZ, one for $h_z(\mathbf{k}) > 0$ and one for $h_z(\mathbf{k}) < 0$. If the radicand is not real, then \mathbb{D} is empty and the Chern numbers are 0. To obtain a nontrivial solution for the Chern numbers, we require the conditions

$$\left(\frac{G}{F} \right)^2 \geq 1 \geq \left(\frac{B}{A} \right)^2, \quad (20)$$

or

$$\left(\frac{B}{A} \right)^2 \geq 1 \geq \left(\frac{G}{F} \right)^2. \quad (21)$$

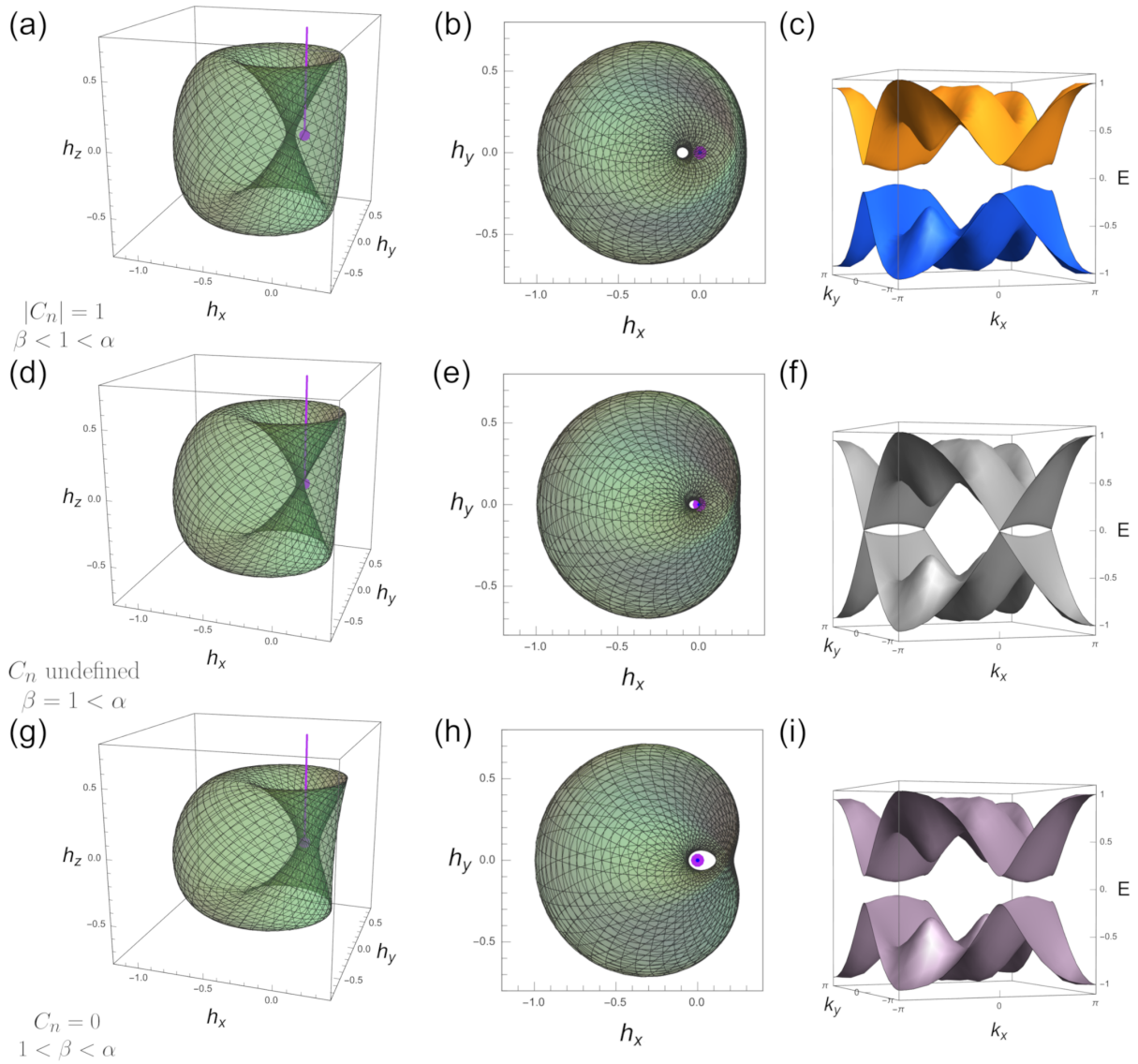


FIG. 2. Topology of the Hamiltonian and band structure. (a) Side and (b) top views of the \mathbf{h} -surface for the model with $\{\alpha, \beta\} = \{\frac{5}{3}, \frac{3}{4}\}$. A $+h_z$ -ray intersects the surface once, corresponding to $|C_1| = 1$. (c) The band structure exhibiting a nontrivial gap; the color of the bands emphasizes the opposite Chern number of the bands. (d-f) The same panels, respectively, for the model with $\{\alpha, \beta\} = \{\frac{5}{3}, 1\}$ and undefined Chern number. The color of the (gapless) bands emphasizes the undefined Chern number. (g-i) The same panels, respectively, for the model with $\{\alpha, \beta\} = \{\frac{5}{3}, \frac{4}{3}\}$ and $C_1 = C_2 = 0$.

The Chern number is undefined if either $n_z(\mathbf{k}) = 0$ or $h_z(\mathbf{k}) = 0$. Otherwise the Chern number is nonzero provided that \mathbb{D} is non-empty. Notice that $n_z(\mathbf{k})$ goes to zero if either $(B/A)^2 = 1$ or $(G/F)^2 = 1$. Hence, the natural parameters of the topological phase diagram are $\alpha = |B/A|$ and $\beta = |G/F|$. For the isotropic model, $\alpha = \beta = 1$; the magnon bands are gapless and C is undefined.

Figure 2(a)-(c) exhibit a nontrivial band topology. For $\alpha = 5/3$ and $\beta = 3/4$, the $+h_z$ -ray intersects the surface once, as seen in Fig. 2(a). The two bands sketched in Fig. 2(c) are gapped and $C_n = \pm 1$. In Figs. 2(d)-(f) with $\alpha = 5/3$ and $\beta = 1$, the surface generated by $\mathbf{h}(\mathbf{k})$ passes

through the origin so the Chern number is undefined. The band structure is then gapless. In Fig. 2(g)-(i) with $\alpha = 5/3$ and $\beta = 4/3$, the $+h_z$ -ray has no intersections with the surface generated by $\mathbf{h}(\mathbf{k})$ due to the presence of a hole. The bands exhibit a trivial gap; $\mathbb{D} = 0$ and $C_n = 0$.

The phase diagram corresponding to these possible cases is shown in Fig. 3. Red lines indicate the cases $\alpha = 1$ or $\beta = 1$ where the Chern numbers are undefined due to a gapless band structure. A red dot indicates the point $\alpha = \beta = 1$ where the model is isotropic. For well-defined Chern numbers of $C_n = 0$ or $C_n = \pm 1$, the band structure is gapped and the material is insulating. Notice

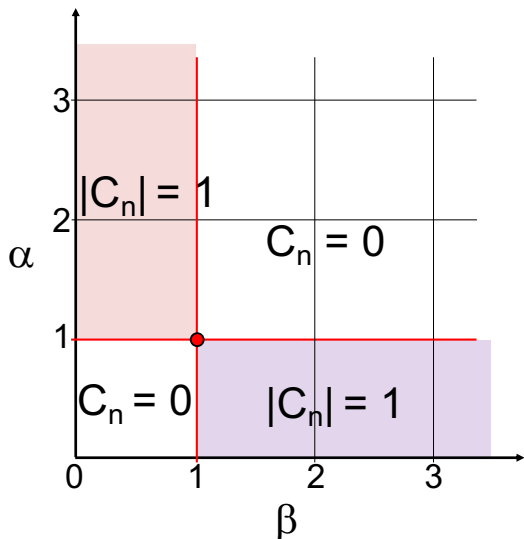


FIG. 3. The phase diagram of the FM zigzag lattice. C_n are undefined along the red lines. The model is isotropic at the red circle with $\alpha = \beta = 1$.

that the phase diagram depends only on the presence of a DM interaction rather than its size, which is not specified in Fig. 3. For any value of D , the retention of the spins along the z -axis can be guaranteed by the easy-axis anisotropy K .

These exact results for the Chern numbers agree with the numerical results obtained in Ref. [30] based on the Berry curvature, given in a semi-classical description by

$$\Omega_n(\mathbf{k}) = \frac{i}{2\pi} \left\{ \frac{\partial}{\partial \mathbf{k}} \times \langle u_n(\mathbf{k}) | \frac{\partial}{\partial \mathbf{k}} | u_n(\mathbf{k}) \rangle \right\} \quad (22)$$

where $|u_n(\mathbf{k})\rangle$ is the Bloch function. The Chern number for band n is then given by

$$C_n = \int_{\text{BZ}} d^2k \Omega_{nz}(\mathbf{k}). \quad (23)$$

It is shown in Ref. [42] that this reduces to Eq. (16) for a two-band model. Based on the analytic solutions for the excitation frequencies given in Eqs. (9) and (10) and the Berry curvature obtained from spin-wave theory, we numerically evaluated the Chern numbers by performing integrals over the first BZ [44]. The numerical results agreed with the exact results derived here and presented in the phase diagram of Fig. 3.

B. Edge modes in pristine and defected ribbons

We now consider the case where a bulk FM zigzag lattice is terminated into a ribbon by making two parallel 45° cuts. Sites lying on the top and bottom edges of the ribbon belong to the same sublattice. An example is sketched in Fig. 4, which shows a ribbon with width

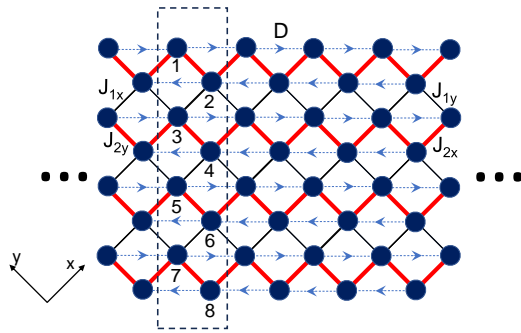


FIG. 4. A ribbon of zigzag width 8 constructed from the FM zigzag lattice. The magnetic unit cell contains the 8 sites indicated within the dashed box.

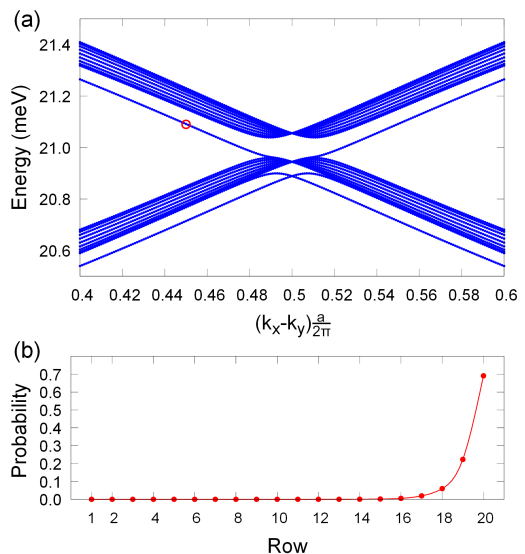


FIG. 5. (a) Magnon bands for a ribbon of width $W = 20$ with $J_{1x} = 0.5$, $J_{1y} = 1.5$, $J_{2x} = 8$, and $J_{2y} = 8$. (b) Probability distribution for the layer occupation of the edge state corresponding to the point marked in (a).

$M = 8$ (8 atomic layers). Notice that the DM interactions lie along the length of the ribbon. The only valid wavevector for the ribbon is $k_x - k_y$ along its length.

The excitation frequencies are evaluated by constructing the Hamiltonian matrix $\underline{H}(\mathbf{k})$ [45], which has dimensions $M \times M$ in the absence of defects. Because $M \gg 1$, the excitation frequencies must be solved by numerically diagonalizing the $M \times M$ matrix $\underline{H}(\mathbf{k})$.

Due to the bulk-boundary correspondence [35–39], the Chern numbers evaluated in the bulk give the number of topological edge modes for the two-dimensional ribbon. As expected, systems with undefined C_n are gapless and do not support edge states along the ribbon. Systems with $C_n = 0$ exhibit a band gap but also have no edge states. Systems with $C_n = \pm 1$ exhibit a gap between

upper and lower bands and also support edge states that connect the upper and lower bands.

We begin by studying a ribbon without defects. Taking $J_{1x} = 0.5$, $J_{1y} = 1.5$, $J_{2x} = 8$, and $J_{2y} = 8$, we have $\alpha = |B/A| < 1$ and $\beta = |G/F| > 1$. Based on the phase diagram of Fig. 3, these values imply that $C_n = \pm 1$. Hence, the system possesses an energy gap and a single state at each edge.

Those predictions are verified in Fig. 5(a), which plots the magnon band energies versus $(k_x - k_y)a/2\pi$ for a ribbon with width $M = 20$. In Fig. 5(b), we plot the layer probability for the edge state that travels around the ribbon with momentum reversed on opposite edges. This probability map verifies that the edge state resides at one edge with swift decay into the bulk of the ribbon.

In order to study the effects of defects, we construct a supercell with W columns of M layers each (W is the supercell width measured along the edge of the ribbon). The Hamiltonian matrix $\underline{H}(\mathbf{k})$ has dimensions $MW \times MW$. We introduce a defect into a supercell with $M = 20$ and $W = 3$. The exchange couplings are the same as in Fig. 5 with the exception that all couplings to the defect site are changed to 40, making the defect attractive so that it preserves the parallel alignment of the spins. This introduces the new mode marked by the green and orange circles in Fig. 6(a). As seen from the probability distribution of Fig. 6(c), this new mode is tightly connected to the defect. As expected, this plot indicates that the topological edge mode is not disturbed by the presence of even a strong defect in the center of the ribbon.

Additionally we introduce a defect into a supercell with $M = 10$ and $W = 5$ at one edge. The exchange couplings are again the same as in Fig. 5 with the exception that all couplings to the defect site at the edge are changed to zero. This introduces new modes seen in Fig. 7(a). As seen from the probability distribution of Fig. 7(b), the defect at the edge does have some effect on the topological edge state; there is additional weight at the second atomic layer instead of a rapid and smooth decay into the ribbon. A closer look at the site-specific probability map in Fig. 7(c) reveals that the topological edge state still primarily resides at the surface, but it explicitly transports around the edge defect by entering the second atomic layer. This strong local perturbation fails to remove the topological edge state even when imposed at the edge.

IV. CONCLUSION

The practical importance of this model is that the topological properties of FM zigzag materials may sensitively depend on strain, which can be used to control the relative anisotropy of the exchange interactions. Suppose, for example, that a pure material has isotropic exchange interactions $J_{1x} = J_{1y} = 2$ meV and $J_{2x} = J_{2y} = 4$ meV. Then $\alpha = \beta = 1$ and the Chern number

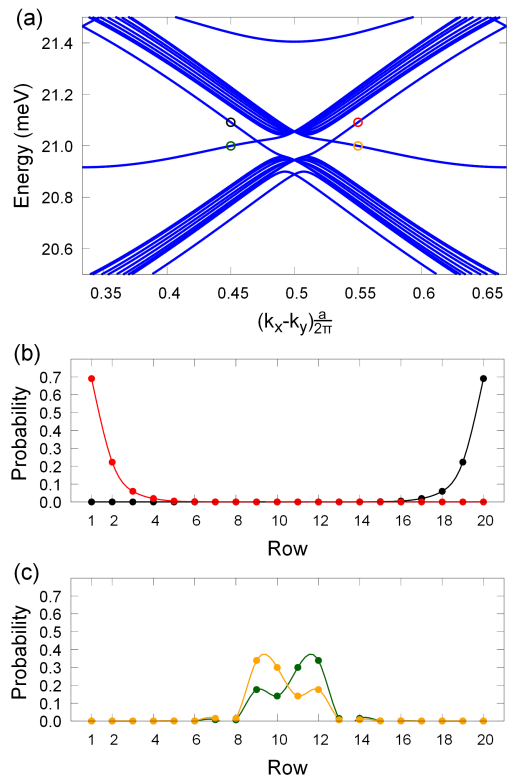


FIG. 6. (a) Magnon bands for a ribbon of size $M = 20$ and $W = 3$ and a point defect in the center of the supercell with $J_{1x} = 0.5$, $J_{1y} = 1.5$, $J_{2x} = 8$, and $J_{2y} = 8$. (b) Probability distribution for the layer occupation of the edge states marked in (a) in black and red. (c) The same, but for the new state localized near the defect marked in (a) in green and orange.

is undefined. A small strain modifying the J_1 exchanges to $J_{1x} = 1.9$ meV and $J_{1y} = 2.1$ meV while leaving J_2 exchanges unchanged would lead to $\alpha = 0.905$ and $\beta = 1.033$, causing $|C_n| = 1$ with an edge mode. A small strain modifying the J_2 exchanges to $J_{2x} = 3.9$ meV and $J_{2y} = 4.1$ meV while leaving J_1 exchanges unchanged would lead to $\alpha = 1.105$ and $\beta = 1.033$, causing $|C_n| = 0$ without an edge mode. A small adjustment to the exchange parameters by strain can turn the topologically protected edge modes on/off entirely.

Remarkably, these topological effects are independent of the size of the DM interaction. Even a small DM interaction is enough to open a gap between the magnon bands when the exchange interactions meet the conditions specified in Fig. 3. Because strain will usually enhance the symmetry breaking that produces the DM interaction, it is likely to increase the size of $|D|$ rather than to suppress it.

To summarize, we have identified analytic conditions for the exchange interactions in an anisotropic FM zigzag model to be a Chern topological insulator with Chern numbers of $C_n = \pm 1$. Because the edge modes of this model are topologically protected from impurities and

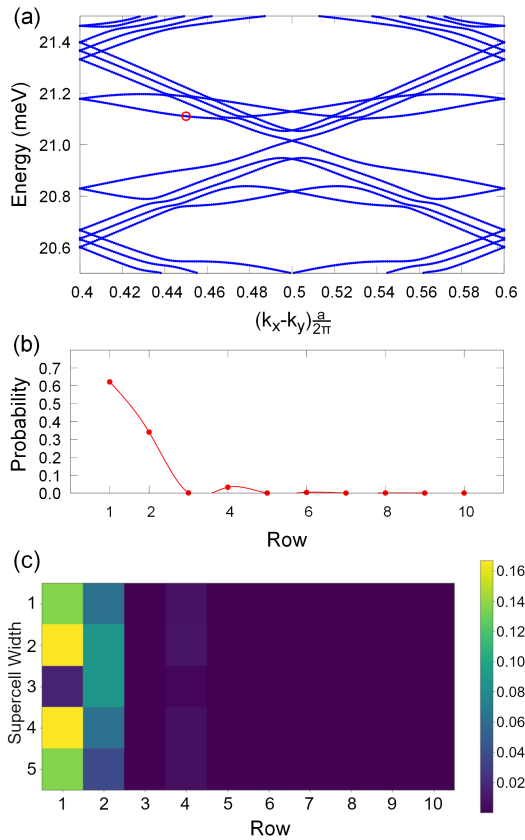


FIG. 7. (a) Magnon bands for a ribbon of size $M = 10$ and $W = 5$ and a point defect at the edge with $J_{1x} = 0.5$, $J_{1y} = 1.5$, $J_{2x} = 8$, and $J_{2y} = 8$. (b) Probability distribution for the layer occupation of the edge state marked in (a) in red. (c) Probability heat map for the same edge state demonstrating its negotiation of the defect.

because the edge modes are sensitive to small changes in the exchange anisotropy, materials that are built on the FM zigzag framework may be important for future technological applications.

ACKNOWLEDGMENTS

We greatly appreciate Dr. Alexander Mook for helpful discussions and constructive criticism during the preparation of the paper. R.F., L.L., and T.B. were sponsored by the U.S. Department of Energy (DOE), Office of Science, Basic Energy Sciences, Materials Sciences and Engineering Division. S.S. was supported in part by the U.S. DOE, Office of Science, Office of Workforce Development for Teachers and Scientists (WDTS) under the Science Undergraduate Laboratory Internships Program (SULI). J.V. acknowledges startup funding from Middle Tennessee State University.

Data Availability Statement

The data that support the findings of this study are available from the authors upon reasonable request.

-
- [1] M. Z. Hasan and C. L. Kane, Colloquium: Topological insulators, *Rev. Mod. Phys.* **82**, 3045 (2010).
 - [2] X.-L. Qi and S.-C. Zhang, Topological insulators and superconductors, *Rev. Mod. Phys.* **83**, 1057 (2011).
 - [3] P. A. McClarty, Topological Magnons: A Review, *Annu. Rev. Condens. Matter Phys.* **13**, 171 (2022).
 - [4] P. A. Pantaleón and Y. Xian, Edge states in a ferromagnetic honeycomb lattice with armchair boundaries, *Physica B: Condens. Matter* **530**, 191 (2018).
 - [5] F. Mei, G. Chen, N. Goldman, L. Xiao, and S. Jia, Topological magnon insulator and quantized pumps from strongly-interacting bosons in optical superlattices, *New J. Phys.* **21**, 095002 (2019).
 - [6] D. Malz, J. Knolle, and A. Nunnenkamp, Topological magnon amplification, *Nature Commun.* **10**, 3937 (2019).
 - [7] L.-c. Zhang, D. Go, J.-P. Hanke, P. M. Buhl, S. Grytsiuk, S. Blügel, F. R. Lux, and Y. Mokrousov, Imprinting and driving electronic orbital magnetism using magnons, *Commun. Phys.* **3**, 227 (2020).
 - [8] S. Fujimoto, Hall Effect of Spin Waves in Frustrated Magnets, *Phys. Rev. Lett.* **103**, 047203 (2009).
 - [9] X. Cao, K. Chen, and D. He, Magnon Hall effect on the Lieb lattice, *J. Phys.: Condens. Matter* **27**, 166003 (2015).
 - [10] F. Zhu, L. Zhang, X. Wang, F. J. dos Santos, J. Song, T. Mueller, K. Schmalzl, W. F. Schmidt, A. Ivanov, J. T. Park, J. Xu, J. Ma, S. Lounis, S. Blügel, Y. Mokrousov, Y. Su, and T. Brückel, Topological magnon insulators in two-dimensional van der Waals ferromagnets CrSiTe_3 and CrGeTe_3 : Toward intrinsic gap-tunability, *Sci. Adv.* **7**, eabi7532 (2021).
 - [11] Y. Onose, T. Ideue, H. Katsura, Y. Shiomi, N. Nagaosa, and Y. Tokura, Observation of the magnon Hall effect, *Science* **329**, 297 (2010).
 - [12] T. Ideue, Y. Onose, H. Katsura, Y. Shiomi, S. Ishiwata, N. Nagaosa, and Y. Tokura, Effect of lattice geometry on magnon Hall effect in ferromagnetic insulators, *Phys. Rev. B* **85**, 134411 (2012).
 - [13] M. Hirschberger, J. W. Krizan, R. J. Cava, and N. P. Ong, Large thermal Hall conductivity of neutral spin excitations in a frustrated quantum magnet, *Science* **348**, 106 (2015).

- [14] M. Hirschberger, R. Chisnell, Y. S. Lee, and N. P. Ong, Thermal Hall effect of spin excitations in a Kagome magnet, *Phys. Rev. Lett.* **115**, 106603 (2015).
- [15] S. Murakami and A. Okamoto, Thermal Hall effect of magnons, *J. Phys. Soc. Jpn* **86**, 011010 (2017).
- [16] R. R. Neumann, A. Mook, J. Henk, and I. Mertig, Thermal Hall effect of magnons in collinear antiferromagnetic insulators: Signatures of magnetic and topological phase transitions, *Phys. Rev. Lett.* **128**, 117201 (2022).
- [17] K.-i. Uchida, H. Adachi, T. Ota, H. Nakayama, S. Maekawa, and E. Saitoh, Observation of longitudinal spin-Seebeck effect in magnetic insulators, *Appl. Phys. Lett.* **97**, 172505 (2010).
- [18] S. M. Wu, W. Zhang, A. KC, P. Borisov, J. E. Pearson, J. S. Jiang, D. Lederman, A. Hoffmann, and A. Bhattacharya, Antiferromagnetic spin Seebeck effect, *Phys. Rev. Lett.* **116**, 097204 (2016).
- [19] M.-C. Chang and Q. Niu, Berry phase, hyperorbits, and the Hofstadter spectrum: Semiclassical dynamics in magnetic Bloch bands, *Phys. Rev. B* **53**, 7010 (1996).
- [20] G. Sundaram and Q. Niu, Wave-packet dynamics in slowly perturbed crystals: Gradient corrections and Berry-phase effects, *Phys. Rev. B* **59**, 14915 (1999).
- [21] D. Xiao, M.-C. Chang, and Q. Niu, Berry phase effects on electronic properties, *Rev. Mod. Phys.* **82**, 1959 (2010).
- [22] M. A. McGuire, H. Dixit, V. R. Cooper, and B. C. Sales, Coupling of crystal structure and magnetism in the layered, ferromagnetic insulator CrI_3 , *Chemistry of Materials* **27**, 612 (2015).
- [23] L. Chen, J.-H. Chung, B. Gao, T. Chen, M. B. Stone, A. I. Kolesnikov, Q. Huang, and P. Dai, Topological spin excitations in honeycomb ferromagnet CrI_3 , *Phys. Rev. X* **8**, 041028 (2018).
- [24] D. G. Joshi, Topological excitations in the ferromagnetic Kitaev-Heisenberg model, *Phys. Rev. B* **98**, 060405 (2018).
- [25] H. Katsura, N. Nagaosa, and P. A. Lee, Theory of the thermal Hall effect in quantum magnets, *Phys. Rev. Lett.* **104**, 066403 (2010).
- [26] S. Owerre, Topological magnon bands in ferromagnetic star lattice, *J. Phys.: Condens. Matter* **29**, 185801 (2017).
- [27] R. Cheng, S. Okamoto, and D. Xiao, Spin Nernst effect of magnons in collinear antiferromagnets, *Phys. Rev. Lett.* **117**, 217202 (2016).
- [28] S. Owerre, Topological honeycomb magnon Hall effect: A calculation of thermal Hall conductivity of magnetic spin excitations, *J. Appl. Phys.* **120**, 043903 (2016).
- [29] R. S. Fishman, Gauge-invariant measure of the magnon orbital angular momentum, *Phys. Rev. B* **107**, 214434 (2023).
- [30] R. S. Fishman, T. Berlijn, J. Villanova, and L. Lindsay, Magnon orbital angular momentum of ferromagnetic honeycomb and zigzag lattice models, *Phys. Rev. B* **108**, 214402 (2023).
- [31] M. Onoda and N. Nishiguchi, $S=1/2$ zigzag-chain structure and ferromagnetism of CdVO_3 , *Journal of Physics: Condensed Matter* **11**, 749 (1999).
- [32] A. A. Tsirlin, O. Janson, and H. Rosner, Unusual ferromagnetic superexchange in CdVO_3 : The role of Cd, *Phys. Rev. B* **84**, 144429 (2011).
- [33] Y. Takano, T. Tsubaki, C. Itoi, K. Takase, and K. Sekizawa, Magnetization and specific heat of a ferromagnetic zigzag spin chain compound LaCrOS_2 , *Solid State Commun.* **122**, 661 (2002).
- [34] L. Duan, X. C. Wang, J. Zhang, Z. Hu, J. F. Zhao, Y. G. Feng, H. L. Zhang, H.-J. Lin, C. T. Chen, W. Wu, Z. Li, R. Wang, J. F. Zhang, T. Xiang, and C. Q. Jin, Synthesis, structure, and magnetism in the ferromagnet La_3MnAs_5 : Well-separated spin chains coupled via itinerant electrons, *Phys. Rev. B* **106**, 184405 (2022).
- [35] R. Matsumoto and S. Murakami, Theoretical prediction of a rotating magnon wave packet in ferromagnets, *Phys. Rev. Lett.* **106**, 197202 (2011).
- [36] R. Matsumoto and S. Murakami, Rotational motion of magnons and the thermal Hall effect, *Phys. Rev. B* **84**, 184406 (2011).
- [37] R. S. K. Mong and V. Shivamoggi, Edge states and the bulk-boundary correspondence in Dirac Hamiltonians, *Phys. Rev. B* **83**, 125109 (2011).
- [38] L. Zhang, J. Ren, J.-S. Wang, and B. Li, Topological magnon insulator in insulating ferromagnet, *Phys. Rev. B* **87**, 144101 (2013).
- [39] A. Mook, J. Henk, and I. Mertig, Magnon Hall effect and topology in Kagome lattices: A theoretical investigation, *Phys. Rev. B* **89**, 134409 (2014).
- [40] G. Pizzi *et al.*, Wannier90 as a community code: new features and applications, *J. Phys.: Condens. Matter* **32**, 165902 (2020).
- [41] S. Coh and D. Vanderbilt, Python Tight Binding (PythTB), Zenodo 10.5281/zenodo.12721315 (2022).
- [42] M. Fruchart and D. Carpentier, An introduction to topological insulators, *Comptes Rendus. Physique* **14**, 779 (2013).
- [43] F. D. M. Haldane, Model for a Quantum Hall Effect without Landau Levels: Condensed-Matter Realization of the “Parity Anomaly”, *Phys. Rev. Lett.* **61**, 2015 (1988).
- [44] R. Shindou, R. Matsumoto, S. Murakami, and J.-i. Ohe, Topological chiral magnonic edge mode in a magnonic crystal, *Phys. Rev. B* **87**, 174427 (2013).
- [45] R. S. Fishman, J. Fernandez-Baca, and T. R  om, *Spin-Wave Theory and its Applications to Neutron Scattering and THz Spectroscopy* (Morgan and Claypool Publishers, San Rafael, 2018).